Electronic Supplementary Information (ESI)

Cr-MOF composited with facet-engineered bimetallic alloys for inducing photocatalytic conversion of CO_2 to C_2H_4

Xiang-Yu Lu, Peng Wang,* Zhao-Feng Qiu and Wei-Yin Sun*

Coordination Chemistry Institute, State Key Laboratory of Coordination Chemistry, School of Chemistry and Chemical Engineering, Nanjing National Laboratory of Microstructures, Collaborative Innovation Center of Advanced Microstructures, Nanjing University, Nanjing 210023, China. E-mail: pengw907@nju.edu.cn (P. Wang); sunwy@nju.edu.cn (W.-Y. Sun)

S1 Materials

All commercially available chemicals and solvents are of reagent grade and were used as received without further purification.

S2 Experimental section

Synthesis of MIL-101(Cr)

In a typical experiment, 104 mg terephthalic acid (H_2BDC) and 250 mg chromic nitrate nonahydrate [$Cr(NO_3)_3 \cdot 9H_2O$] were added to 10 mL of deionized water. After sonicating at ambient temperature for 30 min, the reaction mixture was moved to a Teflon-lined hydrothermal reactor (30 mL) and kept at 180 °C for 15 h. The product was collected as green powder by centrifugation, followed by washing with deionized water and methanol each three times and then dried at 80 °C for 5 h by vacuum.

Synthesis of M-A(111)

100.0 mg MIL-101(Cr) prepared by the above method was dispersed in 10 mL deionized water, followed by addition of 6.3 mg K_2PtCl_4 and 2.2 mg Na_2PdCl_4, and stirred continuously for 6 h

to give a green suspension. Next, 16.6 mg polyvinylpyrrolidone (PVP, MW = 24,000) and 0.4 mL of formaldehyde solution (40%) were added. The pH value of the solution was adjusted to about 4 by adding drops of 1 : 1 HCl solution and the total volume of the solution was kept at 15 mL. The mixed solution was transferred to a 30 mL Teflon-lined stainless steel autoclave and sealed. The autoclave was then heated at 180 °C for 2 h before it was cooled down to room temperature. The black nanoparticles were centrifuged with importing 15 mL of acetone-ethanol mixture (1:1 in v/v) and washed alternately with ethanol and water three times.

Synthesis of M-A(100)

100.0 mg MIL-101(Cr) prepared by the above method was dispersed in 10 mL deionized water, followed by addition of 6.3 mg K_2PtCl_4 and 2.2 mg Na_2PdCl_4, and stirred continuously for 6 h to give a green suspension. Next, 50 mg PVP, 180 mg KBr and 0.9 mg KI were added. The pH value of the solution was adjusted to about 3 by adding drops of 1 : 1 HCl solution and the total volume of the solution was kept at 15 mL. The mixed solution was transferred to a 30 mL Teflon-lined stainless steel autoclave and sealed. The autoclave was then heated at 160 °C for 4 h before it was cooled down to room temperature. The black nanoparticles were centrifuged with importing 45 mL of acetone and further washed alternately with ethanol and cyclohexane three times.

Photocatalytic CO_2 reduction measurements

The photocatalytic CO_2 reduction was carried out in a closed gas-solid reaction system (Labsolar-6A, Beijing Perfectlight) equipped with a circulating water filter to avoid the photothermal effect. 2 mg of the catalyst was dispersed in 1.0 mL of isopropanol, then uniformly dispersed on a glass fiber film (Φ47 mm, pore size 0.22 μm) and dried appropriately, then fixed in the reactor with 2 mL ultrapure water. After the overall system was vacuumed three times, the high-purity CO_2 (99.999%) was introduced into the reactor. The 300 W Xenon lamp is used as a light source, using an analog sunlight (AM 1.5) cutoff filter with an intensity

of 300 mW cm^{-2} and maintaining the light for 4 h. The generated products were monitored using a gas chromatograph (GC9720 II) equipped with two flame ionization detectors (FID) for C_2H_4, CO and CH_4 monitoring and one thermal conductivity detector (TCD) for H_2 detection.

S3 Characterization methods

Powder X-ray diffraction (PXRD) data were collected on a Bruker D8 Advance X-ray diffractometer with Cu Kα (λ=1.5418 Å) radiation. FT-IR ATR spectra within 4000-400 cm^{-1} were recorded on an infrared spectrophotometer (Bruker Tensor II) with a diamond ATR module. X-ray photoelectron spectroscopy (XPS) was performed on Thermo ESCALAB 250XI with aluminum Kα radiation. Scanning electron microscopy (SEM) images were obtained on a Hitachi S-4800 SEM at 5 kV. Transmission electron microscopy (TEM) and high-resolution transmission electron microscopy (HRTEM) images were achieved on JEM-2100 with an acceleration voltage of 100 kV. The high-angle annular dark-field scanning transmission electron microscopy (HAADF-STEM) images and STEM-EDX elemental mappings were collected on FEI Talos F200X (Thermo Fisher Scientific). UV-vis diffuse reflectance spectra (DRS) were recorded on a Shimadzu UV-3600 spectrophotometer in the wavelength range of 200 - 800 nm, and a white standard $BaSO_4$ was used as a reference. Photoluminescence (PL) spectra were measured on a Perkin Elmer LS-55 fluorescence spectrophotometer. Time-resolved fluorescence decay spectra were obtained at room temperature on a HORIBA Jobin Yvon FL-3 spectrometer. Transient photocurrent responses were performed using a CHI730E electrochemical workstation (Chen Hua Instrument, Shanghai, China). The electrochemical impedance spectroscopy (EIS) and Mott-Schottky tests were performed on the Zahner electrochemical workstation (IM6ex, Zahner Scientific Instruments, German). Inductively coupled plasma mass spectrometry (ICP-MS) data were recorded on Aglient 7700X.

S4 Electrochemical tests

5.0 mg catalysts and 20 μL of Nafion (Du Pont) were added into 1 mL isopropanol to prepare

ink through ultrasonic processing for preparing the working electrode. A standard three-electrode system with a Pt wire as the counter electrode and an Ag/AgCl as the reference electrode was used. A 0.2 M Na_2SO_4 solution was used as the electrolyte. The electrochemical impedance spectroscopy (EIS) was performed on the Zahner electrochemical workstation with photocatalyst-coated carbon paper as a working electrode, which was prepared by dropping the above ink (200 μL) onto the surface of the carbon paper and dried at 100 ºC. The measurements were carried out with a bias potential of -0.1 V with a frequency range from 10^{-2} to 10^5 Hz under a nitrogen atmosphere. Photocurrent measurements were recorded on the CHI 730E electrochemical workstation with a photocatalyst-coated ITO as a working electrode, prepared with the above method. The measurements were carried out under chopped light at 0.5 V.

S5 *In situ* FT-IR measurements

In situ FT-IR measurements were conducted using the Thermo Fisher is50 FT-IR spectrometer equipped with an *in situ* diffuse reflectance cell (Harrick). First, 2 mg photocatalyst was vacuum treated, and then CO_2 was introduced into a reactor containing 2 mL ultrapure water and adsorbed in the dark for 30 min. After that, the photocatalyst was irradiated for 60 min, and FT-IR spectra were recorded repeatedly at an interval of 10 min.

S6 Computational method.

All density functional theory (DFT) calculations were carried out using the Vienna ab initio simulation package (VASP) based on the projector augmented wave (PAW) method.[1-3] Within the generalized gradient approximation (GGA), the Perdew-Burke-Ernzerhof (PBE), a popular exchange-correlation functional, was employed in geometry optimizations. The PtPd surfaces were modeled with 2×2 supercells with a lattice constant of 3.90*3.90*3.87 Å. Two metal layers were used for {111} surface and four metal layers were used for {100} surface. During the structure optimization, the adsorbate and one top layer were allowed to relax in all directions while the other layers were fixed at the optimized bulk positions. The relaxations of the atoms

were carried out with the quasi-Newton minimization scheme, until the maximum force on any atom was below 0.05 eV $Å^{-1}$. Ionic cores were described by PAW potentials. The vertical separation between successive slabs was in all cases more than 15 Å and dipole corrections were applied. The search for optimal geometries was performed using a cut-off for the plane-wave basis set of 450 eV. The Brillouin zones of all surfaces were sampled with 4×4×1 Monkhorst-Pack grids. The Fermi levels of surfaces with and without adsorbed species were smeared by the Methfessel-Paxton approach with a Gaussian width of 0.2 eV, and all energies were extrapolated to T = 0 K. Molecules were calculated with a width of 0.01 eV and Gaussian smearing was used instead.

To study the CO_2RR pathway, we built a model in periodic boundary condition (PBC) with the primitive cell. The Grimme method was also applied to take the long-range dispersion interaction into consideration. The kinetic energy cutoff for the plane-wave expansion was set to 400 eV and a 1×1×1 sheet k-point mesh was used. The energy convergence value between two consecutive steps was chosen as 1×10^{-5} eV, and a maximum force was set to be lower than 0.04 eV/Å on each atom. The CO_2 reduction process can be described by the following steps:

$$*CO + H^+ + e^- \rightarrow *CHO \quad (1)$$

$$*CHO + H^+ + e^- \rightarrow *OCH_2 \quad (2)$$

$$*OCH_2 + H^+ + e^- \rightarrow *OCH_3 \quad (3)$$

$$*CH_3 + H^+ + e^- \rightarrow *O + CH_4 \quad (4)$$

The asterisk * represents the adsorption over the sites. The values for the free energies of each gaseous and adsorbed species are calculated by:

$$G = E_{total} + E_{ZPE} - TS \quad (4)$$

E_{total} is the total energy from the DFT calculations. E_{ZPE} is the zero-point energy, S is the entropy, and T is the temperature.

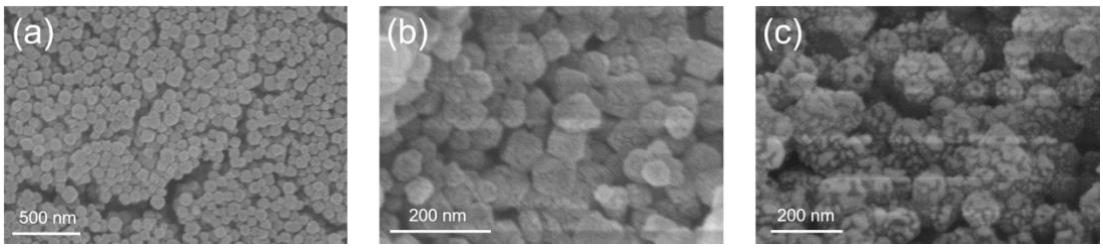

Fig. S1 SEM images of (a) MIL-101(Cr); (b) M-A(111); (c) M-A(100).

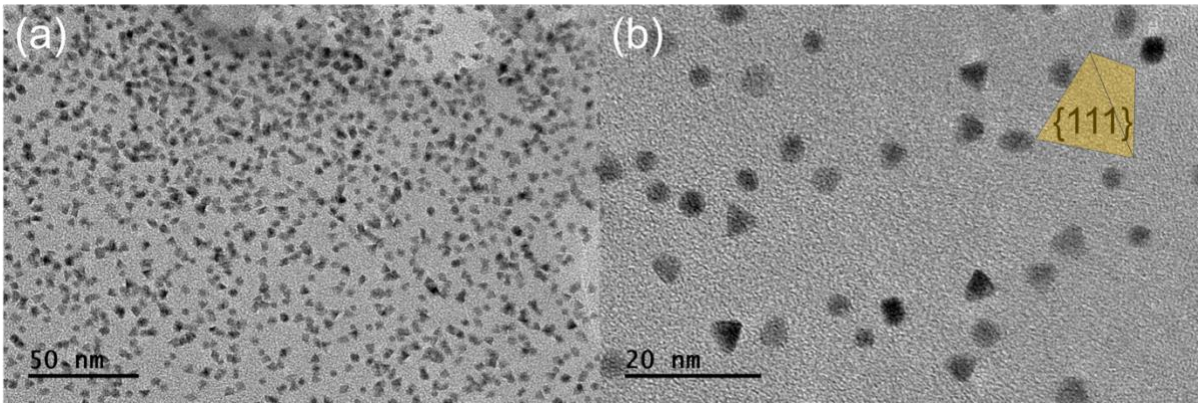

Fig. S2 (a) TEM and (b) HRTEM images of PPNA with exposed {111} facets. The inset illustrates a schematic representation of the PPNA(111) structure.

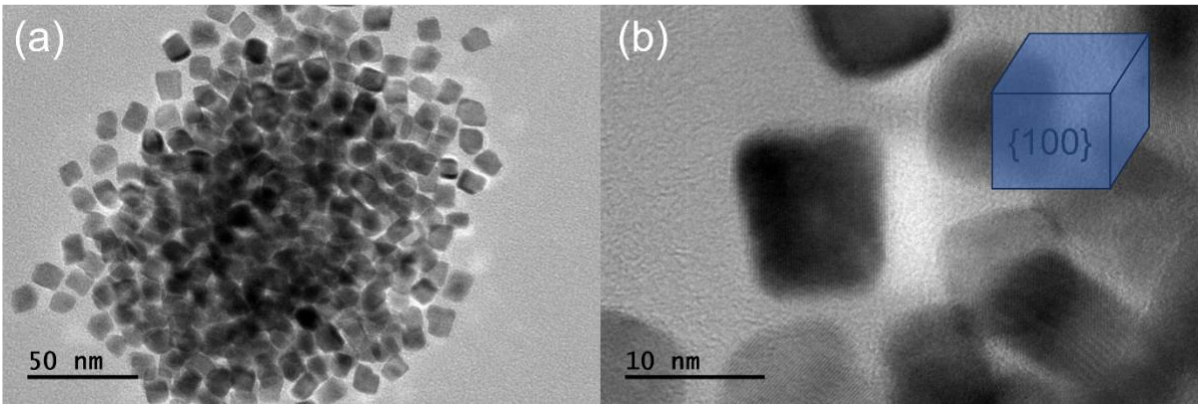

Fig. S3 (a) TEM and (b) HRTEM images of PPNA with exposed {100} facets. The inset illustrates a schematic representation of the PPNA(100) structure.

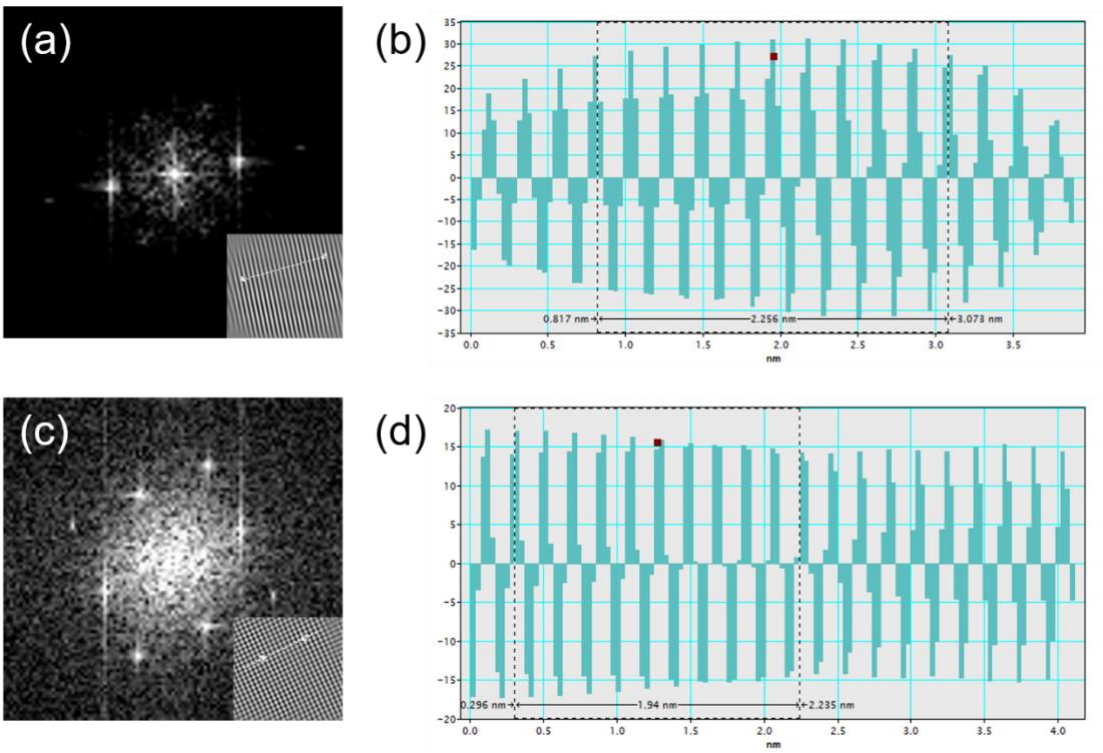

Fig. S4 (a) FFT image of PPNA(111), the illustration is a mathematical image obtained by the inverse Fourier transform; (b) particle size distribution obtained in the viewfinder frame. The average lattice spacing is 0.225 nm by the ten-point method. (c) FFT image of PPNA(100), the illustration is a mathematical image obtained by the inverse Fourier transform; (d) particle size distribution obtained in the viewfinder frame. The average lattice spacing is 0.194 nm by the ten-point method.

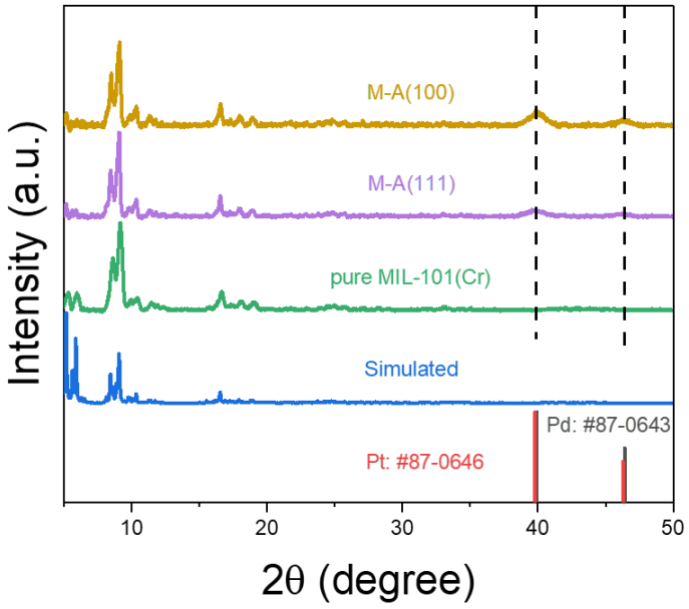

Fig. S5 PXRD patterns of varied catalysts.

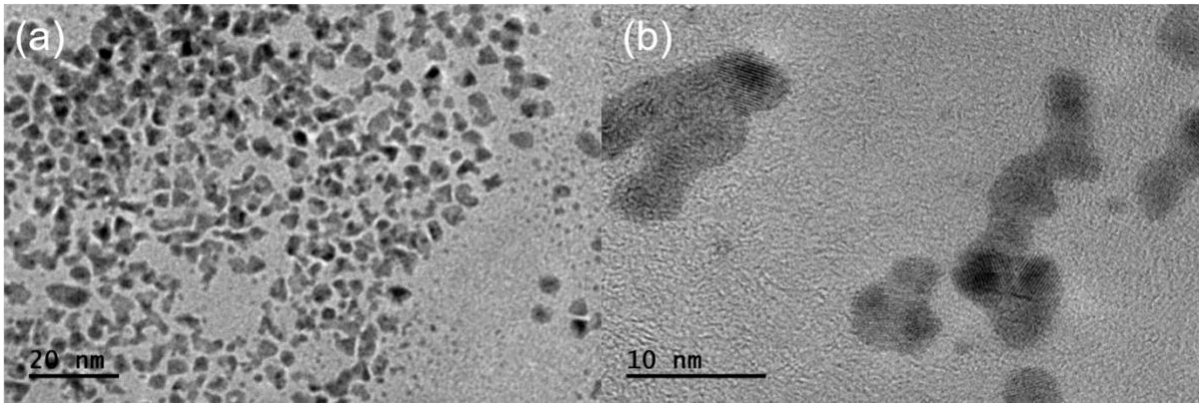

Fig. S6 (a) TEM image and (b) HRTEM image of M-A(111) synthesized at 160 °C.

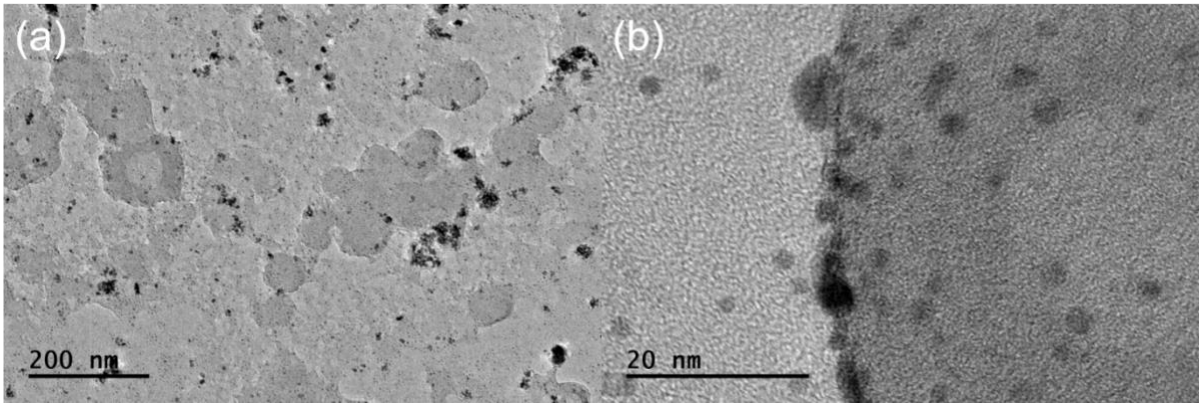

Fig. S7 (a) TEM image and (b) HRTEM image of M-A(111) synthesized using ascorbic acid as the reducing agent.

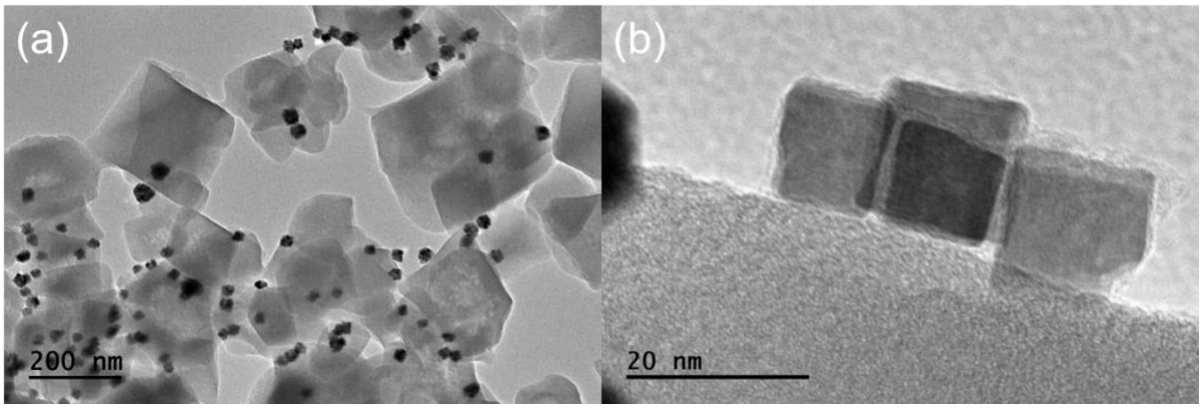

Fig. S8 (a) TEM image and (b) HRTEM image of M-A(100) synthesized without the addition of KBr and KI.

As shown in the above Figs. S6-S8, under reaction conditions at 160 °C for the {111} growth, the uniform tetrahedral structure of PPNA failed to form. Instead, a spherical morphology was observed, indicating a loss of ordered facet exposure. This demonstrates that temperature is a critical parameter in the growth process of PPNA. When ascorbic acid was used as the reducing agent instead of formaldehyde, significant PPNA aggregation occurred, along with partial degradation of MIL-101(Cr). For the {100} growth, in the absence of KBr and KI during the reaction, the resulting PPNA exhibits poor dispersion, which may be due to excessive particle affinity, leading to large cuboidal aggregates rather than well-dispersed PPNA particles.

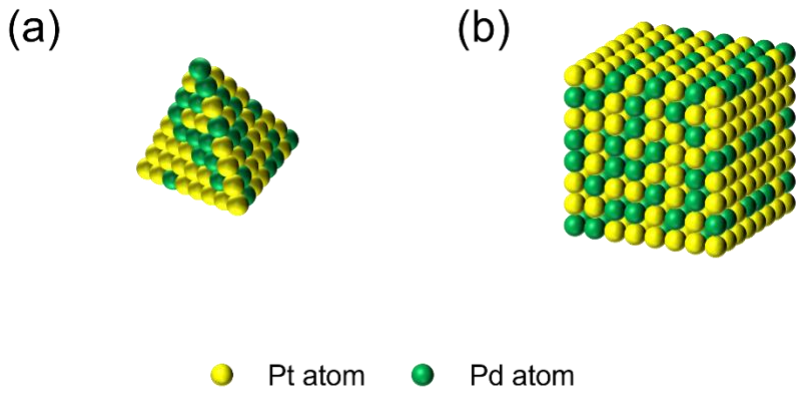

Fig. S9 Atomic packing diagrams for (a) PPNA(111) and (b) PPNA(100).

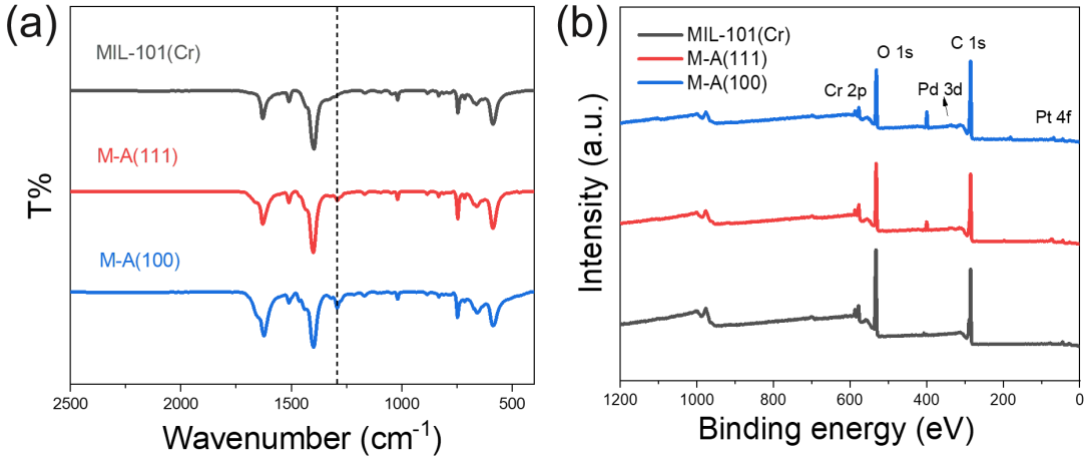

Fig. S10 FT-IR (a) and XPS survey (b) spectra of varied catalysts.

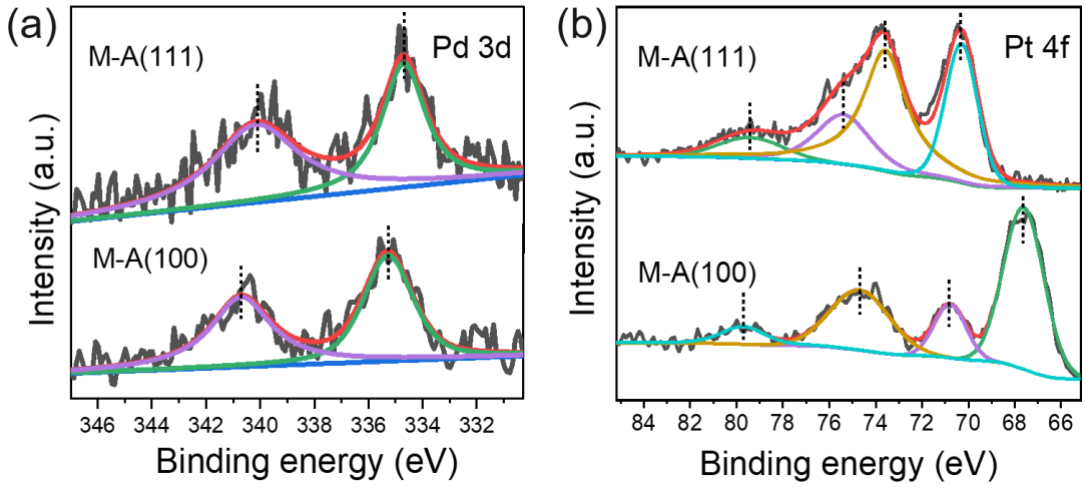

Fig. S11 High-resolution Pd 3d (a) and Pt 4f (b) XPS spectra of M-A(111) and M-A(100).

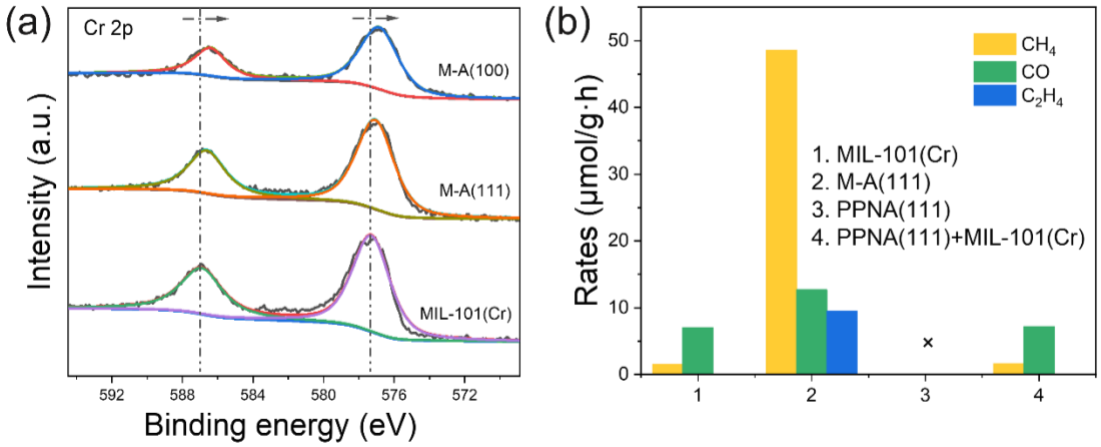

Fig. S12 (a) High-resolution Cr 2p XPS spectra of various catalysts; (b) photocatalytic CO_2 reduction performance of PPNA(111) and control samples.

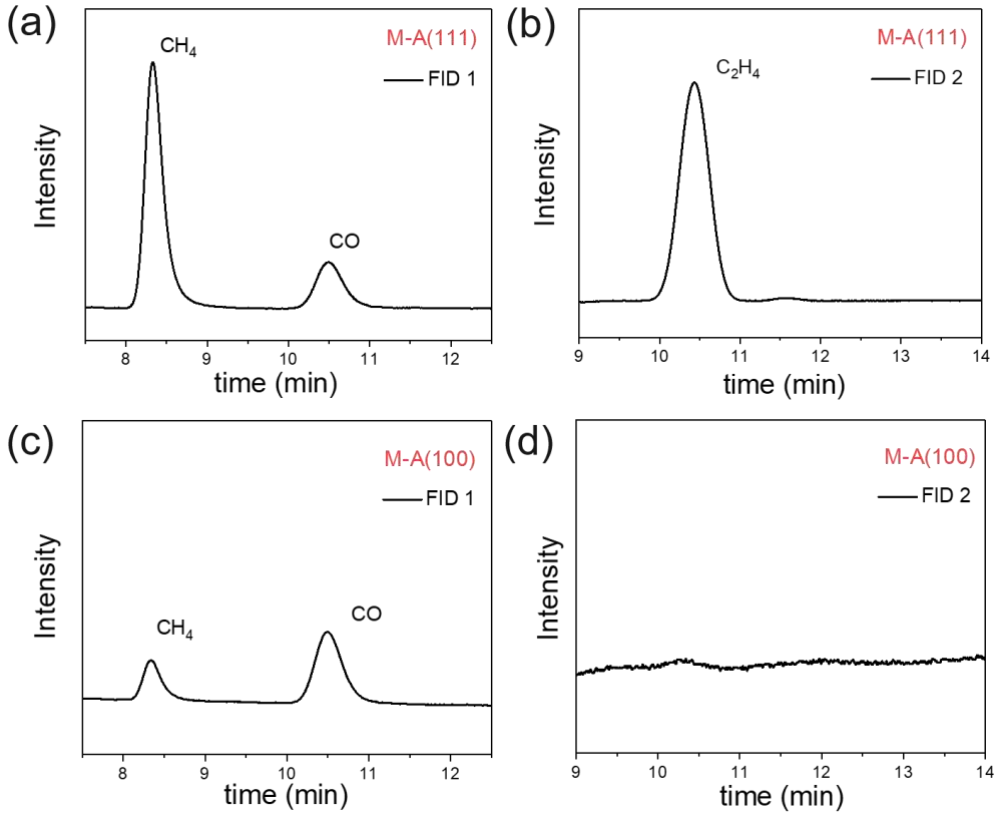

Fig. S13 Typical gas chromatogram observed during the irradiation: (a) FID1 detector for CH_4 and CO monitoring in M-A(111); (b) FID2 detector for C_2H_4 monitoring in M-A(111); (c) FID1 detector for CH_4 and CO monitoring in M-A(100); (d) FID2 detector for C_2H_4 monitoring in M-A(100).

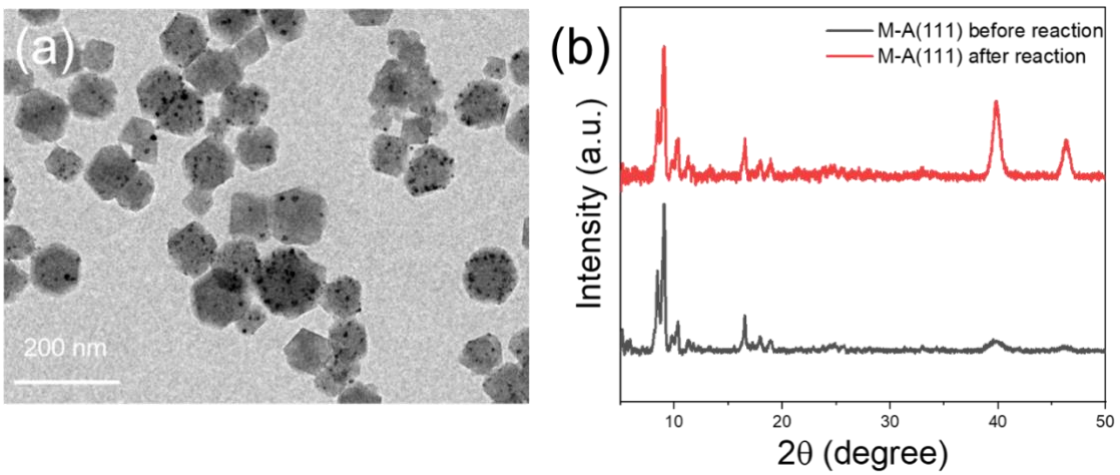

Fig. S14 (a) TEM image of M-A(111) after cyclic test; (b) PXRD patterns. The enhancement in the intensity after cyclic test in Fig. S14b may be due to the increased exposure of the alloy nanoparticles and partial agglomeration after the cyclic test as observed in Fig. S14a.

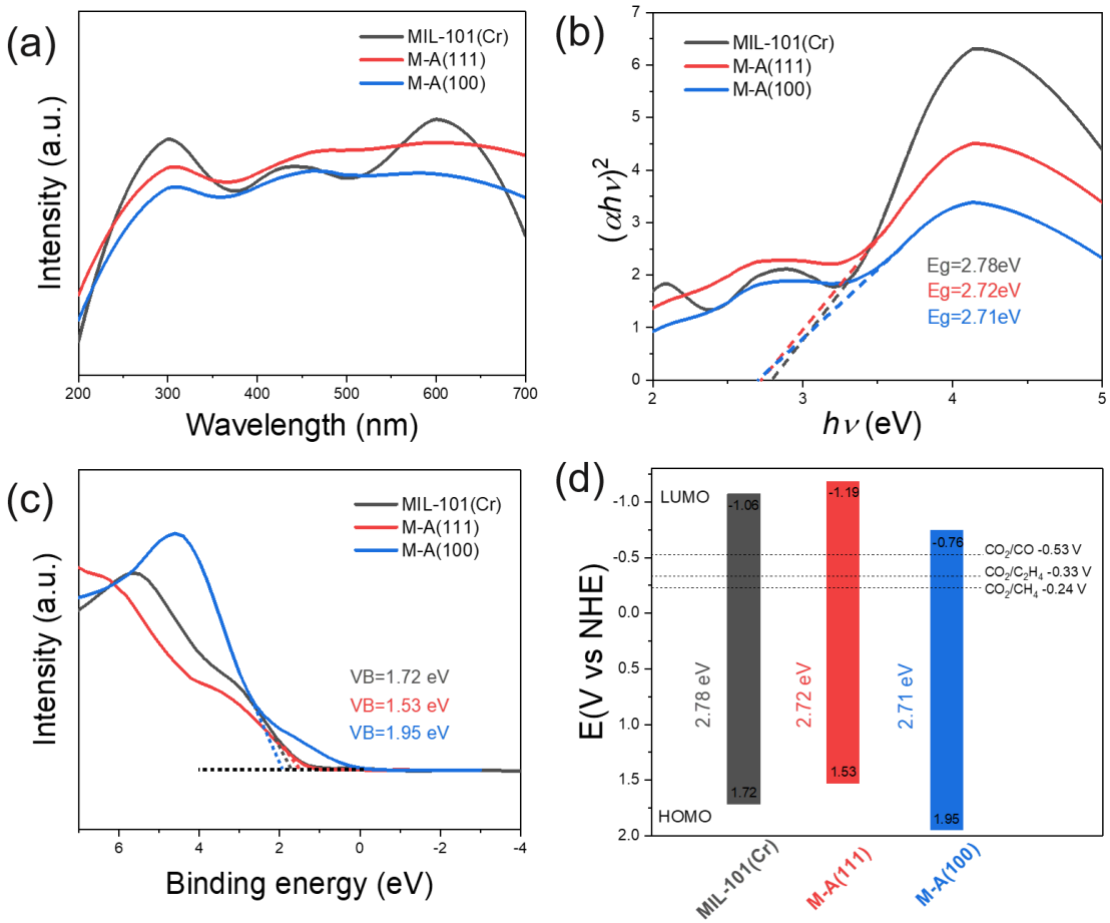

Fig. S15 (a) UV−vis diffuse reflectance spectra; (b) corresponding Tauc plots; (c) XPS valence band spectra; (d) HOMO−LUMO diagram of the varied catalysts.

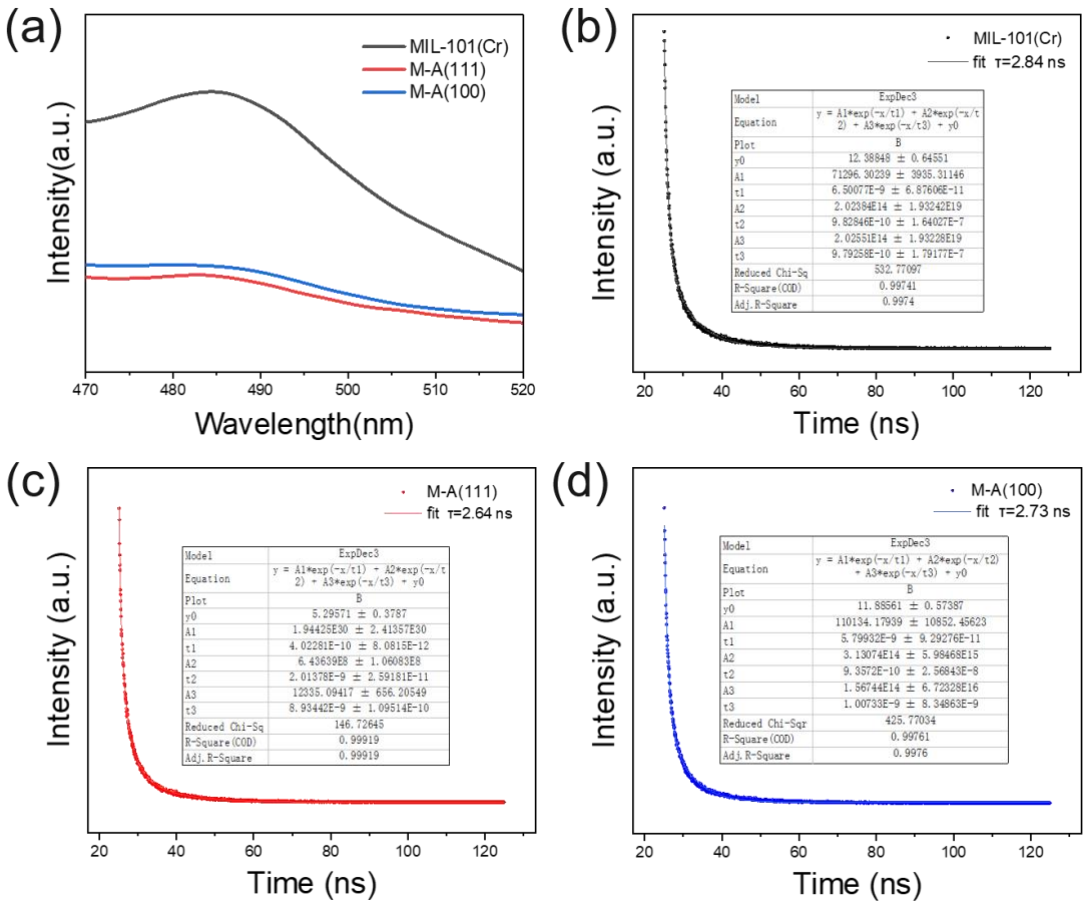

Fig. S16 (a) Photoluminescence of varied catalysts and time-resolved fluorescence decay spectra of (b) MIL-101(Cr); (c) M-A(111) and (d) M-A(100).

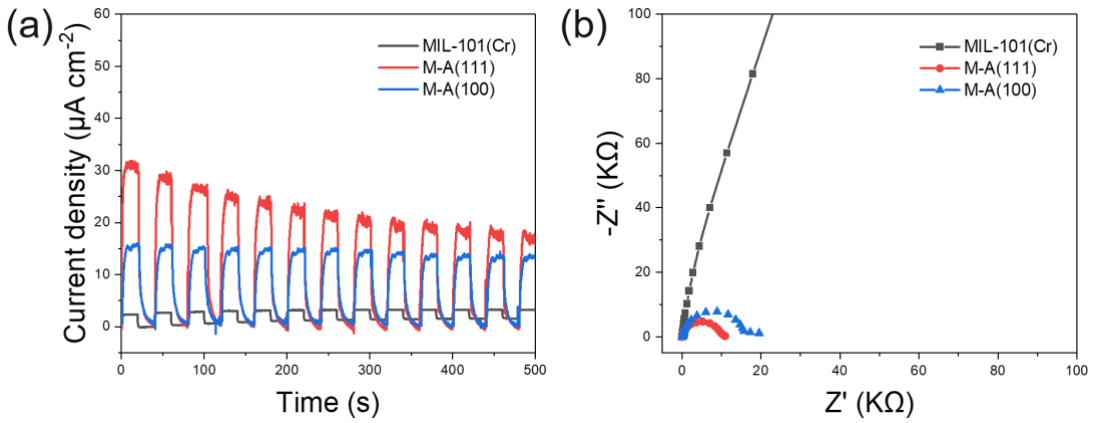

Fig. S17 (a) Transient photocurrent response and (b) EIS Nyquist plots for varied catalysts.

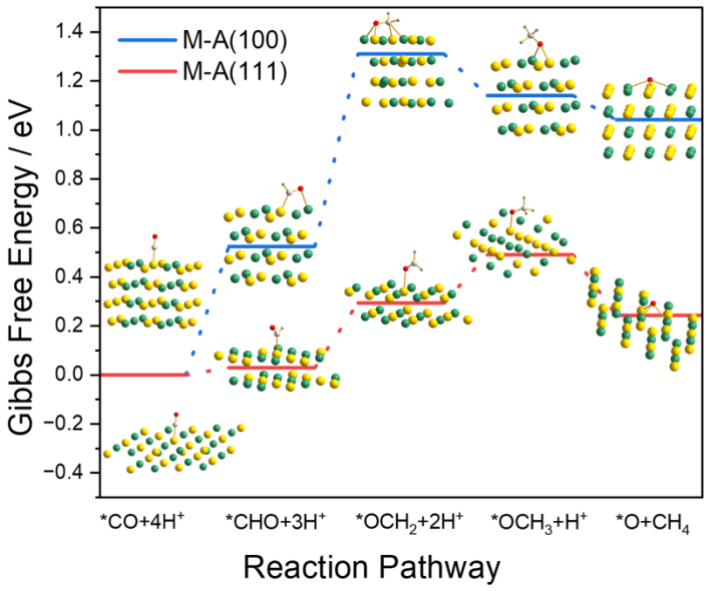

Fig. S18 Calculated reaction pathway and reaction intermediates for *CO-to-CH_4 conversion at 0 V versus RHE (pH = 0).

According to the DFT calculations, it can be concluded that {111} surface is the more favorable for CO_2-to-CH_4 conversion than the {100} one, and the rate-determining step for the conversion is the hydrogenation of CO species.

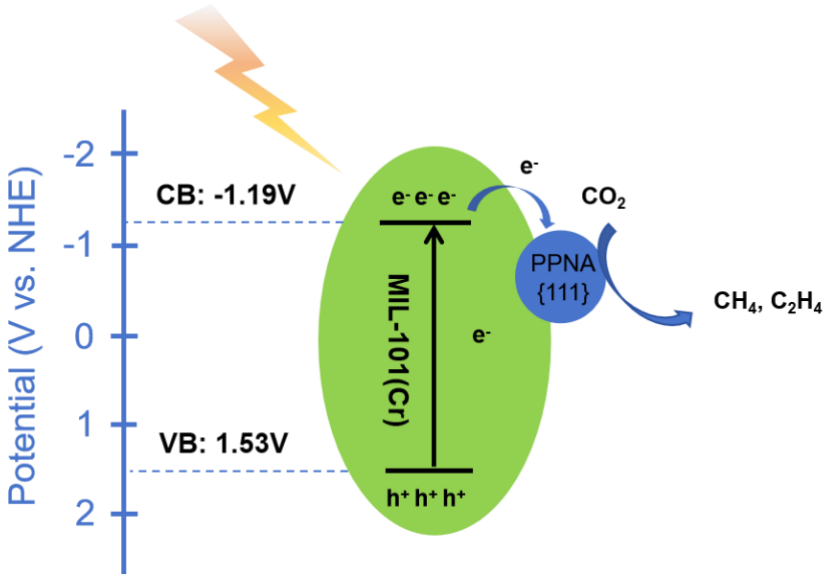

Scheme S1 Schematic illustration of CO_2 reduction photocatalyzed by PPNA(111) on MIL-101(Cr).

References

1. Perdew, J. P.; Burke, K.; Ernzerhof, M. *Phys. Rev. Lett*., 1996, **77**, 3865–3868.

2. Vanderbilt, D. *Phys. Rev. B,* 1990, **41**, 7892–7895.

3. Monkhorst, H. J.; Pack, J. D. *Phys. Rev. B,* 1976, **13**, 5188– 5192.